Impact of a modified convective scheme on the Madden-Julian Oscillation and El Niño–Southern Oscillation in a coupled climate model

Xiaoqing Wu,[1] Liping Deng,[1] Xiaoliang Song,[1] Guido Vettoretti,[2] W. Richard Peltier,[2] and Guang Jun Zhang[3]

Received 9 May 2007; revised 6 July 2007; accepted 3 August 2007; published 30 August 2007.

[1] The connection between the intraseasonal Madden-Julian Oscillation (MJO) and interannual El Niño–Southern Oscillation (ENSO) has been proposed and investigated for the last two decades. However, many fully coupled atmosphere-ocean general circulation models (GCMs) are still unable to simulate many important characteristics of these two phenomena partly due to the great uncertainty in the representation of subgrid-scale cloud systems. We report herein the simulation of an El Niño in a fully coupled GCM with a modified convection scheme, which captures many of the observed features of the 1997/1998 El Niño event. The representation of convection in the coupled model plays a major role in modeling both interannual ENSO and intraseasonal MJO variability in closer accord with observations, and in reproducing the evolution of 1997/1998 El Niño-type events. **Citation:** Wu, X., L. Deng, X. Song, G. Vettoretti, W. R. Peltier, and G. J. Zhang (2007), Impact of a modified convective scheme on the Madden-Julian Oscillation and El Niño–Southern Oscillation in a coupled climate model, *Geophys. Res. Lett.*, *34*, L16823, doi:10.1029/2007GL030637.

1. Introduction

[2] The simulation of El Niño-Southern Oscillation (ENSO) in fully coupled atmosphere-ocean general circulation models (GCMs) is currently one of the leading problems in modeling large scale tropical dynamics [e.g., *Zhang et al.*, 2001; *AchutaRao and Sperber*, 2006; *Deser et al.*, 2006]. This modeling deficiency exists in many modern GCMs despite great progress that has been made in observing the genesis and evolution of the phenomenon [e.g., *McPhaden*, 1999], advances in modeling ENSO with intermediate coupled models [e.g., *Cane and Zebiak*, 1985], and the development of various theories that have been proposed to explain the characteristics of ENSO [e.g., *Neelin et al.*, 1998]. Part of the difficulties arises from the great uncertainty in the treatment of convection, clouds, and cloud-radiation interaction in GCMs. Cloud systems affect large-scale circulation and wave disturbances through the release of latent heat; the redistribution of heat, moisture and momentum; the reflection, absorption and emission of radiation; and precipitation. The large-scale forcing in turn influences and modulates the development and organization of convection and clouds. The coupling of convective processes with the large-scale dynamics is crucial for modeling the global distribution of precipitation and the Madden-Julian Oscillation (MJO) [e.g., *Zhang*, 2005]. The impact of the MJO upon Tropical Pacific variability in coupled models may also play an important role in the simulation of ENSO [e.g., *Lau*, 1985]. However, how these two phenomena with widely different timescales (intraseasonal and interannual) interact with each other is still unknown, partly due to the lack of skill of fully coupled GCMs in simulating both the MJO and ENSO [e.g., *Zhang et al.*, 2001].

2. Modifications to the Convection Scheme

[3] The understanding and modeling of cloud systems in response to the evolving large-scale circulation has improved in the last decade due to the development of cloud-resolving models (CRM)s and long-term field experiments including GATE (Global atmospheric research program Atlantic Tropical Experiment), TOGA COARE (Tropical Ocean Global Atmosphere - Coupled Ocean Atmosphere Response Experiment), and ARM (Atmospheric Radiation Measurement) [e.g., *Moncrieff et al.*, 1997; *Grabowski et al.*, 1996; *Wu et al.*, 1998]. The knowledge gained from observational and CRM studies helps us advance the parameterization schemes of convection, clouds, and cloud-radiation interaction used in large scale coupled models [e.g., *Zhang*, 2002; *Wu et al.*, 2003; *Zhang and Wu*, 2003; *Wu and Liang*, 2005]. Three major changes are implemented into the *Zhang and McFarlane* [1995] convection scheme in the National Center for Atmospheric Research Climate System Model with improved tropical dynamics (NCAR CSM 1.4 T31AL18:3x3OL25 [*Boville and Gent*, 1998; *Otto-Bliesner and Brady*, 2001]).

[4] 1. The revised closure assumption, based on the observations from ARM and TOGA COARE and implemented in CCM3 by *Zhang* [2002], relates convection to the destabilization of the tropospheric layer above the planetary boundary layer by the large-scale processes. The cloud base mass flux is determined by the CAPE change due to the large-scale temperature and moisture advection.

[5] 2. The trigger condition for deep convection, based upon results from cloud-resolving simulations, allows the activation of deep convection when the CAPE increase due to the large-scale forcing exceeds 70 J kg^{-1} h^{-1}.

[6] 3. The convective momentum transport (CMT) parameterization [*Zhang and Cho*, 1991], validated and

[1]Department of Geological and Atmospheric Sciences, Iowa State University, Ames, Iowa, USA.
[2]Department of Physics, University of Toronto, Toronto, Ontario, Canada.
[3]Scripps Institution of Oceanography, La Jolla, California, USA.

0094-8276/07/2007GL030637$05.00

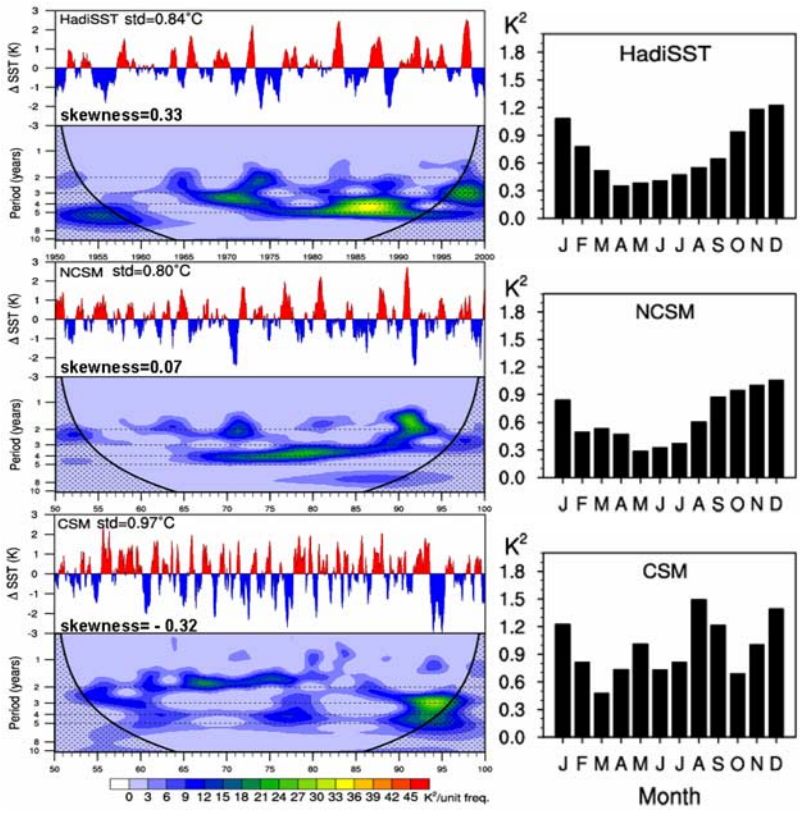

Figure 1. (left) Monthly time series of the Niño-3.4 SST anomaly and wavelet power spectrum analysis and (right) monthly averaged variances from observations of the Hadley Centre Sea Ice and SST dataset (HadISST,1950–1999 [*Rayner et al.*, 2003]), CSM1.4 at resolution T31 with the modified convection scheme (NCSM, years 50–99), and standard CSM1.4 at T31 (CSM, years 50–99). Standard deviations (std) and skewness of each time series are included.

simplified through the study of cloud-resolving simulations [*Wu et al.*, 2002; *Zhang and Wu*, 2003] and implemented in CCM3 by *Wu et al.* [2003, 2007], redistributes the horizontal momentum through the subsidence compensating convective mass flux, detrainment of in-cloud momentum and cloud-scale perturbation pressure gradient. The interaction between CMT and the thermodynamic effects of convection plays an important role in improving tropical convection and the Hadley circulation.

[7] The CSM1.4 is a previous version of the NCAR Community Climate System Model version 3 (CCSM3), which shares basically the same convection scheme. The CSM1.4 is less expensive when compared with the CCSM3 at the same horizontal and temporal resolutions, and is widely used by paleoclimate groups. Despite the use of different ocean, sea ice and land models and the modifications to the cloud and radiation schemes in the CCSM3, the CCSM3 still suffers from the same long standing problems as the CSM1.4 such as double ITCZ problem, poor simulations of MJO and ENSO etc. It will be naturally a next step to investigate how the improved convection scheme interacts with other components in the CCSM3.

3. Coupled Climate Simulations

[8] A100-year simulation is conducted using CSM1.4 with the modified convection scheme (NCSM), and compared with the standard CSM1.4 simulation (CSM) and observations. Both simulations used fixed modern boundary conditions and radiative trace gas forcing (CO_2 = 355 ppmv). Current efforts to compare Tropical Pacific variability in coupled GCM simulations with 20th century observations is unlikely to capture the observed variability unless the simulation is forced by 20th century natural variability. It has been demonstrated in previous studies that ENSO variability can be influenced by external variations such as solar variability and volcanic activity [*Adams et al.*, 2003; *Mann et al.*, 2005]. The 20th century observed ENSO variability may also be influenced by the 20th century anthropogenic signal but this impact upon ENSO variability is still under current investigation [*Collins and the CMIP Modeling Groups*, 2005]. The simulations in this study are standard CSM runs without the forcing of 20th century time-dependent atmospheric sulfur, greenhouse gases, and solar variability when compared with observations.

[9] Figure 1 shows the time series and wavelet power spectrum analysis of 50-year monthly sea surface temperature (SST) anomaly over the Niño-3.4 region (5°N–5°S, 170°–120°W). It is clear that much of the high frequency interannual variability simulated in the CSM has been reduced in the NCSM and is in better agreement with observations from 1950–2000. The amplitude of the variability measured by the standard deviation is reduced from 0.97°C in the CSM to 0.80°C in the NCSM which is comparable with 0.84°C measured from observations. The improvement of variability in the NCSM can also be

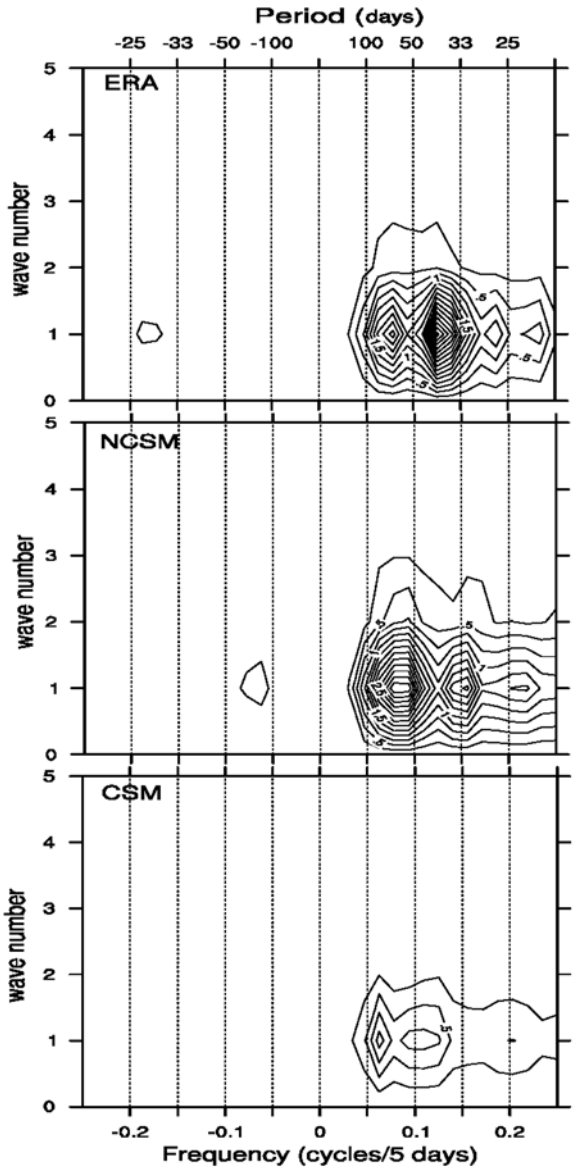

Figure 2. Wave number-frequency spectra of 200-hPa velocity potential averaged between 10°N and 10°S for ERA (ECMWF Re-Analysis)-40 reanalysis (years 1989–1998), the NCSM (years 80–89) and the CSM (years 80–89). The contour starts from 0.25×10^{11} m^4 s^{-2} with the interval of 0.25×10^{11} m^4 s^{-2}. Positive (negative) frequency and period represent the eastward (westward) propagation. A 20–100-day band-pass filter is applied to remove the annual cycle and lower frequencies in the pentad time series. The averaged spectrum is derived from individual spectra that are 64 pentads in length overlapping each other by 10 pentads [*Maloney and Hartmann*, 2001].

assessed by measuring the skewness of the SST anomaly distribution, which provides a measure of the relative strength of El Niño events versus La Niña events. The SST anomalies in the CSM have a distribution that is negatively skewed (−0.32, stronger La Niñas), while the observations have an almost opposite positive skewness (0.33, stronger El Niños). The NCSM has a slightly positive skewness (0.07, slightly stronger El Niños), which is a significant improvement when compared with observations. The wavelet analysis provides an estimate of the irregular ENSO frequency during the 50 years with the CSM displaying the majority of the variance in power in a 2–3 year band, while the NCSM displays power more prominently in a 4-year band in the middle of the 50 year segment. The observations have the majority of ENSO power concentrated in a 4–5 year band in the second half of the 20th century.

[10] The seasonal variation of the standard deviation of the SST anomaly time series (Figure 1, right) further supports the improvement of ENSO simulation upon implementation of the modified convection scheme into the CSM. While the CSM fails to simulate the seasonal cycle of the variability, the NCSM correctly produces the minimum variability during May–July and the maximum during November–January and is in agreement with observations although the variability during winter (December–February) is weaker than is observed. Inspection by eye between the three time-series, wavelet spectrums, and statistical measures clearly demonstrate that the NCSM is simulating ENSO in much closer accord with the observations than in the CSM.

[11] To examine the intraseasonal variability of the coupled simulations, ten-year (years 80–89) daily model outputs of velocity potential at 200 hPa were saved and used to perform a wave number-frequency spectrum analysis. The intraseasonal power of the NCSM is significantly enhanced as compared with the CSM and closer to the power which is observed (Figure 2). Both the NCSM and the observed spectra show a peak of power at wave number 1 and an eastward period of 64 days. The observed power spectrum also has a secondary peak at 40 days, while the NCSM has a secondary peak at 32 days. It is an encouraging result that the coupled GCM with the modified convection scheme is able to improve the simulation of both ENSO and the MJO phenomena with very different timescales.

[12] With this improved tropical climate variability, the NCSM is able to replicate an El Niño event similar in character to the 1997/1998 El Niño. Figure 3 shows the temporal and spatial evolution of daily SSTs and 850 hPa zonal wind anomalies together with the time series of the MJO index. A two-year model period (July year 89-July year 91) is compared with a two-year observed period (July 1996–July 1998) demonstrating a striking similarity between the two time series. The El Niño event is characterized by positive SST anomalies that had developed in the eastern and central Pacific between March of 1997 (year 90 in the NCSM) and June of 1998 (year 91), accompanied by the appearance of westerly wind anomalies and the collapse of trade winds in the lower troposphere and surface. Before the onset of the event, negative SST anomalies (cold tongue) had occupied the eastern Pacific and extended westward to the central Pacific. The westerly wind anomalies then developed over the Indian Ocean and the western Pacific. The MJO index displays increased MJO activity in both the observations (in November 1996 and April 1997) and the NCSM simulation (in October year 89 and March year 90). After the onset, westerly wind anomalies, triggered by MJO activity, had propagated across the entire Pacific to the west coast of South America and ignited downwelling equatorial Kelvin waves which then led to the

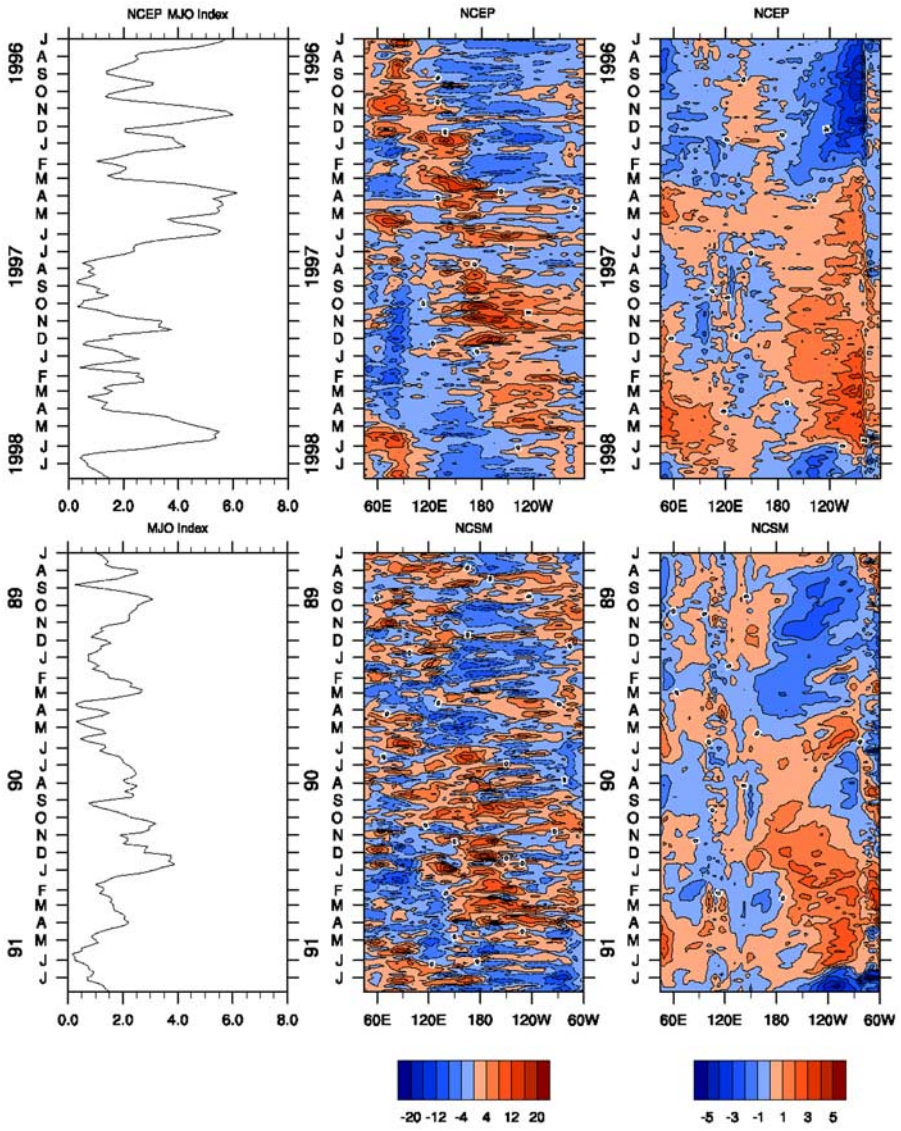

Figure 3. Temporal-spatial evolution of (middle) pentad 850-hPa zonal wind anomalies (m s^{-1}) and (right) SST anomalies (°C) averaged between 2°N and 2°S and (left) time series of pentad MJO index for observations (NCEP, July 1996–July 1998, top), and the NCSM (July year 89-July year 91, bottom). Anomalies are with respect to the mean over the two-year period. To get the MJO index, a band-passed 20–100-day band-pass filter is applied to 850-hPa stream function field (50°N to 50°S). A space-time extended empirical orthogonal function (EEOF) analysis is then used to get the dominant modes. Each mode of EEOF has a set of substructures which represent the time lags at −10 day, −5 day, 0 day, +5 day, +10 day. With the first two dominant EEOF modes, the MJO index is obtained as the square root of the sum of the squares of the two principle components (EEOF-1 and EEOF-2) [*Lau*, 2005].

deepening of the thermocline in the eastern Pacific as shown by the 20°C isotherm depth anomalies in the ocean and corresponding positive ocean heat content anomalies (not shown). Before the onset of El Niño, positive ocean heat content and positive 20°C isotherm depth anomalies had built up over the western Pacific west of the date line.

[13] The onset of MJO activity in April 1997 (March year 90) and the appearance of westerly wind anomalies enhanced atmosphere-ocean interactions and forced the warm ocean water anomalies in the western Pacific to propagate eastward and upward to the eastern Pacific which then led to the onset of El Niño (not shown). While the El Niño was in its mature stage, after December 1997 (December year 90), easterly wind anomalies had developed over the western Pacific and forced the shoaling of the thermocline (negative 20°C isotherm depth anomalies). The cold water anomalies then propagated eastward and upward to the eastern Pacific, which subsequently led to the sudden termination of the El Niño (not shown).

[14] Several theories have been proposed to explain the nature of ENSO including the delayed oscillator [e.g., *Suarez and Schopf*, 1988; *Battisti and Hirst*, 1989], the recharge-discharge of equatorial ocean heat content [*Jin*, 1997] and stochastic forcing hypotheses [e.g., *Lau*, 1985; *Penland and Sardeshmukh*, 1995; *Moore and Kleeman*, 1999]. The new coupled simulation presented in this report

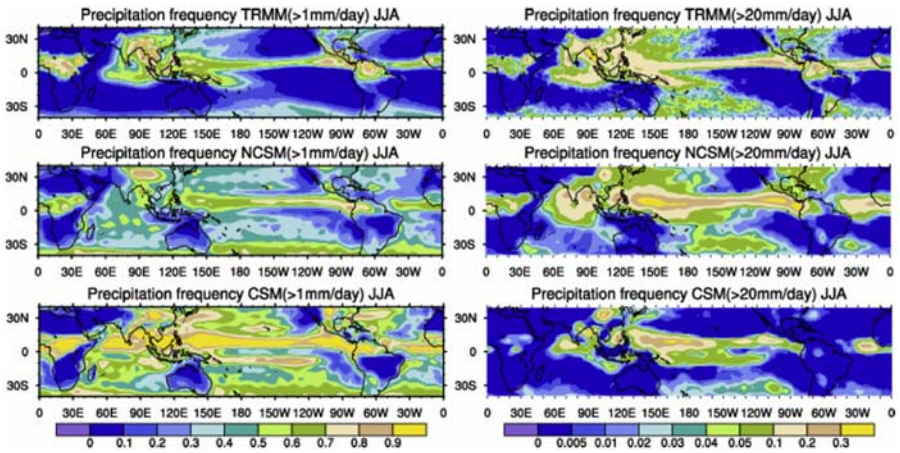

Figure 4. JJA (June, July and August) daily precipitation (>1 mm day^{-1}, left; >20 mm day^{-1}, right) frequencies (%) from (top) TRMM (Tropical Rainfall Measuring Mission) 3B42 satellite observations (1998–2003), (middle) the NCSM (years 80–89), and (bottom) the CSM (years 80–89).

suggests that the representation of deep convection holds the key for explaining the genesis, development and termination of an El Niño event through atmosphere-ocean coupling. Figure 4 displays the frequency distribution of precipitation larger than 1 mm day^{-1} over JJA (June, July and August) of the 10-year (years 80–89) period. The NCSM clearly rains much less frequently as compared with the CSM over the Indian Ocean, the Pacific and the Atlantic, and is in closer agreement with the TRMM satellite observations over the 6-year (years 1998–2003) period. Also of interest is the measure of the frequency of heavy precipitation (larger than 20 mm day^{-1}), which is higher in the NCSM than in the CSM. The NCSM produces more heavy precipitation over North, Central and South America, the Indian Ocean and the Western Pacific. Most coupled GCMs share a similar problem characterized by the overestimation of light precipitation and the underestimation of heavy precipitation in these regions [e.g., *Dai*, 2006]. This deep convection can be considered as a measure of the stochastic forcing in the model. In the standard CSM, the stochastic forcing is added too frequently and too weakly, which resulted in weak intraseasonal variability. With the modified scheme in the NCSM, the stochastic forcing is less frequent but stronger, which resulted in increased MJO activity. This increased activity then acts as a more coherent stochastic forcing that affects the ocean circulation through the enhancement of westerly wind anomalies and the development of El Niño. The development of easterly wind anomalies due to the cold SST anomalies over the western Pacific during the peak of an El Niño event has the opposite effect on the ocean circulation with resulting upwelling Kelvin waves and the termination of El Niño as the cold ocean water anomalies propagate eastward and upward to the eastern Pacific and the ocean surface.

[15] **Acknowledgments.** We thank Eric Maloney for providing the FORTRAN code used for the spectral analysis in Figure 2 and Chidong Zhang, Mike Chen, and Ronghua Zhang for their comments. Computing support by Daryl Herzmann is greatly appreciated. This research was supported by the Office of Science (BER), U.S. Department of Energy, grants DE-FG02-04ER63868 and DE-FG02-03ER63532.

References

AchutaRao, K., and K. R. Sperber (2006), ENSO simulation in coupled ocean-atmosphere models: Are the current models better?, *Clim. Dyn.*, *27*, 1–15.

Adams, J. B., M. E. Mann, and C. M. Ammann (2003), Proxy evidence for an El Niño-like response to volcanic forcing, *Nature*, *426*, 274–278.

Battisti, D. S., and A. C. Hirst (1989), Interannual variability in the tropical atmosphere–ocean system: Influence of the basic state, ocean geometry, and nonlinearity, *J. Atmos. Sci.*, *46*, 1687–1712.

Boville, B. A., and P. R. Gent (1998), The NCAR climate system model, version one, *J. Clim.*, *11*, 1115–1130.

Cane, M. A., and S. E. Zebiak (1985), A theory for El Niño and the Southern Oscillation, *Science*, *228*, 1084–1087.

Collins, M., and the CMIP Modeling Groups (2005), El Niño or La Niña-like climate change, *Clim. Dyn.*, *24*, 89–104.

Dai, A. (2006), Precipitation characteristics in eighteen coupled climate models, *J. Clim.*, *19*, 4605–4630.

Deser, C., A. Capotondi, R. Saravanan, and A. Phillips (2006), Tropical Pacific and Atlantic climate variability in CCSM3, *J. Clim.*, *19*, 2451–2481.

Grabowski, W. W., X. Wu, and M. W. Moncrieff (1996), Cloud resolving modeling of tropical cloud systems during Phase III of GATE. Part I: Two-dimensional experiments, *J. Atmos. Sci.*, *53*, 3684–3709.

Jin, F. F. (1997), An equatorial ocean recharge paradigm for ENSO. part 1: Conceptual model, *J. Atmos. Sci.*, *54*, 811–829.

Lau, K.-M. (1985), Elements of a stochastic-dynamical theory of the El Niño/Southern Oscillation, *J. Atmos. Sci.*, *42*, 1552–1558.

Lau, W. K. M. (2005), El Niño–Southern Oscillation connection, in *Intraseasonal Variability in the Atmosphere-Ocean Climate System*, edited by W. K. M. Lau and D. E. Waliser, 271–305, Springer, Berlin.

Maloney, E. D., and D. L. Hartmann (2001), The sensitivity of intraseasonal variability in the NCAR CCM3 to changes in convective parameterization, *J. Clim.*, *14*, 2015–2034.

Mann, M. E., M. A. Cane, S. E. Zebiak, and A. Clement (2005), Volcanic and solar forcing of the Tropical Pacific over the past 1000 years, *J. Clim.*, *18*, 447–456.

McPhaden, M. J. (1999), Genesis and evolution of the 1997–98 El Niño, *Science*, *283*, 950–954.

Moncrieff, M. W., S. K. Krueger, D. Gregory, J.-L. Redelsperger, and W.-K. Tao (1997), GEWEX Cloud System Study (GCSS) Working Group 4: Precipitating convective cloud systems, *Bull. Am. Meteorol. Soc.*, *78*, 831–845.

Moore, A. M., and R. Kleeman (1999), Stochastic forcing of ENSO by the intraseasonal oscillation, *J. Clim.*, *12*, 1199–1220.

Neelin, J. D., D. S. Battisti, A. C. Hirst, F. F. Jin, Y. Wakata, T. Yamagata, and S. E. Zebiak (1998), ENSO theory, *J. Geophys. Res.*, *103*, 14,261–14,290.

Otto-Bliesner, B., and E. C. Brady (2001), Tropical Pacific variability in the NCAR climate system model, *J. Clim.*, *14*, 3587–3607.

Penland, C., and P. D. Sardeshmukh (1995), The optimal growth of tropical sea surface temperature anomalies, *J. Clim.*, *8*, 1999–2024.

Rayner, N. A., D. E. Parker, E. B. Horton, C. K. Folland, L. V. Alexander, D. P. Rowell, E. C. Kent, and A. Kaplan (2003), Global analyses of sea

surface temperature, sea ice, and night marine air temperature since the late nineteenth century, *J. Geophys. Res.*, *108*(D14), 4407, doi:10.1029/2002JD002670.

Suarez, M., and P. Schopf (1988), A delayed action oscillator for ENSO, *J. Atmos. Sci.*, *45*, 3283–3287.

Wu, X., and X. Liang (2005), Effect of subgrid cloud-radiation interaction on climate simulations, *Geophys. Res. Lett.*, *32*, L24806, doi:10.1029/2005GL024432.

Wu, X., W. W. Grabowski, and M. W. Moncrieff (1998), Long-term behavior of cloud systems in TOGA COARE and their interactions with radiative and surface processes. Part I: Two-dimensional modeling study, *J. Atmos. Sci.*, *55*, 2693–2714.

Wu, X., M. W. Moncrieff, X.-Z. Liang, and G. J. Zhang (2002), Evaluation and impact study of convective momentum parameterization using 3D cloud-resolving model and general circulation model, paper presented at 25th Conference on Hurricanes and Tropical Meteorology, Am. Meteorol. Soc., San Diego, Calif., 29 April to 3 May.

Wu, X., X. Liang, and G. J. Zhang (2003), Seasonal migration of ITCZ precipitation across the equator: Why can't GCMs simulate it?, *Geophys. Res. Lett.*, *30*(15), 1824, doi:10.1029/2003GL017198.

Wu, X., L. Deng, X. Song, and G. J. Zhang (2007), Coupling of convective momentum transport with convective heating in global climate simulations, *J. Atmos. Sci.*, *64*, 1334–1349.

Zhang, C. (2005), Madden-Julian Oscillation, *Rev. Geophys.*, *43*, RG2003, doi:10.1029/2004RG000158.

Zhang, C., H. H. Hendon, W. S. Kessler, and A. Rosati (2001), A workshop on the MJO and ENSO, *Bull. Am. Meteorol. Soc.*, *82*, 971–976.

Zhang, G. J. (2002), Convective quasi-equilibrium in midlatitude continental environment and its effect on convective parameterization, *J. Geophys. Res.*, *107*(D14), 4220, doi:10.1029/2001JD001005.

Zhang, G. J., and H. R. Cho (1991), Parameterization of the vertical transport of momentum by cumulus clouds. part I: Theory, *J. Atmos. Sci.*, *48*, 1483–1492.

Zhang, G. J., and N. A. McFarlane (1995), Sensitivity of climate simulations to the parameterization of cumulus convection in the Canadian Climate Centre general circulation model, *Atmos. Ocean*, *33*, 407–446.

Zhang, G. J., and X. Wu (2003), Convective momentum transport and perturbation pressure field from a cloud-resolving model simulation, *J. Atmos. Sci.*, *60*, 1120–1139.

L. Deng, X. Song, and X. Wu, Department of Geological and Atmospheric Sciences, Iowa State University, 3010 Agronomy Hall, Ames, IA 50011, USA. (wuxq@iastate.edu)

W. R. Peltier and G. Vettoretti, Department of Physics, University of Toronto, Toronto, ON, Canada M5S 1A7.

G. J. Zhang, Scripps Institution of Oceanography, La Jolla, CA 92093, USA.